

# A novel biomass gasification process for the generation of inherently separated syngas using the concept of chemical looping technology

Haochen Sun <sup>a,b</sup>, Zhiqing Wang <sup>a,\*</sup>, Hengyang Miao <sup>a,b</sup>, Zheyu Liu <sup>a</sup>, Jiejie Huang <sup>a</sup>, Jin Bai <sup>a</sup>, Chengmeng Chen <sup>c</sup>, Yitian Fang <sup>a,\*</sup>

<sup>a</sup> State Key Laboratory of Coal Conversion, Institute of Coal Chemistry, Chinese Academy of Sciences, Taiyuan 030001, China

<sup>b</sup> University of Chinese Academy of Sciences, Beijing 100049, China

<sup>c</sup> CAS Key Laboratory of Carbon Materials, Institute of Coal Chemistry, Chinese Academy of Sciences, Taiyuan 030001, China



## ARTICLE INFO

### Keywords:

Partial oxidation of char  
Hydrogen generation  
Ferrites  
 $\text{BaFe}_2\text{O}_4$   
Inherent separation of syngas

## ABSTRACT

Biomass-based hydrogen generation has been showing a potential prospect in solving the global environment and energy challenges. This study introduces a novel chemical looping system, known as chemical looping partial oxidation and hydrogen generation (CLPH) process, which can generate inherently separated syngas from biomass, thus presenting a good application prospect. The feasibility of this system and the selection of appropriate oxygen carriers (OCs), which were the key to the success of this system, were investigated in this work. Four  $\text{MFe}_2\text{O}_4$  ( $\text{M}=\text{Ni, Co, Ca, Ba}$ ) OCs were chosen according to the modified Ellingham diagram, and their performances as well as the reaction pathway of  $\text{BaFe}_2\text{O}_4$  and C were comprehensively investigated. The results show that all OCs exhibit a good solid-solid reactivity, but the CO selectivity of  $\text{CaFe}_2\text{O}_4$  and  $\text{BaFe}_2\text{O}_4$  (around 60%) are higher than that of  $\text{CoFe}_2\text{O}_4$  and  $\text{NiFe}_2\text{O}_4$  (around 20%). Additionally, the cycle performance of  $\text{CaFe}_2\text{O}_4$  is worse than that of  $\text{BaFe}_2\text{O}_4$ , which is owing to the poor self-healing property. Thus,  $\text{BaFe}_2\text{O}_4$  was chosen as the ideal OC for the CLPH process. A successful biomass gasification process for the generation of inherently separated syngas was developed, achieving a carbon conversion rate of 93%, CO selectivity of  $\geq 60\%$ , wonderful hydrogen yield of  $\geq 1700 \text{ mL/g}$ -biomass char and hydrogen purity of  $\geq 94\%$  over 5 cycles.

## 1. Introduction

With the continuous improvement of industrialization and living standards of modern society, global energy demand has been steadily increasing during the past several decades [1], and the utilization of fossil-based energy has resulted in severe environmental problems [2]. Besides that, the Paris Agreement has proposed a maximum increase of  $1.5^\circ\text{C}$  in global temperature to reduce its influence on climate change [3]. Thus, more and more attentions have been paid on the utilization of renewable energy.

Biomass is considered as a potential alternative to fossil fuels due to its abundance, renewability and nearly zero carbon emissions [4]. Meanwhile, hydrogen, being clean and with minimal adverse effects on environment [5,6], is anticipated to become the most important energy, essential for the global energy structure in the future. Therefore, it is imperative to convert biomass into hydrogen. Gasification, serving as a thermo-conversion process capable of effectively converting carbonaceous fuel into gaseous fuel (CO, H<sub>2</sub>), has shown a good prospect for

biomass-based hydrogen generation. However, the traditional biomass gasification requires gasifying agents such as oxygen-rich air and high-temperature steam to obtain high quality of syngas [7], and it always encounters the problems of N<sub>2</sub> dilution, undesired CO<sub>2</sub>, tar generation and so on [8].

In recent years, chemical looping technology has developed rapidly. This technology introduces oxygen carrier (OC) into the redox system, circulating it between two or three reactors to transfer oxygen atoms. As a result, fuel doesn't directly contact with air, thus avoiding the problem of N<sub>2</sub> dilution and enabling the generation of high purity of CO<sub>2</sub> at the outlet of the fuel reactor [9–12]. Moreover, unlike gas-phase oxygen, the introduced OC can only provide lattice oxygen, which prefers to partially oxidize rather than fully oxidize the fuel [13], while partial oxidization is the most important feature of gasification, making chemical looping technology suited very well to the gasification process. Consequently, more and more chemical looping gasification process was proposed. Zhen Huang et al. [14] comprehensively investigate the biomass direct chemical looping (BDCL) conversion process with natural

\* Corresponding authors.

E-mail addresses: [qcumt@sxicc.ac.cn](mailto:qcumt@sxicc.ac.cn) (Z. Wang), [fyt@sxicc.ac.cn](mailto:fyt@sxicc.ac.cn) (Y. Fang).

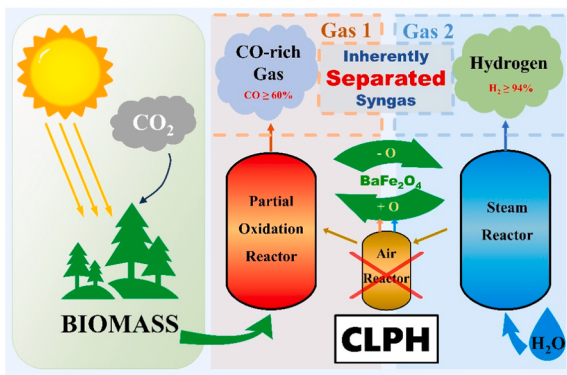


Fig. 1. Flow diagram of the proposed CLPH process.

hematite as OC and they found that the gas yield and carbon conversion rate increased from  $0.75 \text{ Nm}^3/\text{kg}$  and 62.23% to  $1.06 \text{ Nm}^3/\text{kg}$  and 87.63% when OC was introduced. Fang He et al. [15] investigated the performances of  $\text{NiFe}_2\text{O}_4$  OC during chemical looping gasification (CLG) process with different  $\text{H}_2\text{O}/\text{CO}_2$  addition, the results showed that this system can generate bio-syngas with flexible  $\text{H}_2$  to  $\text{CO}$  ratios, and the generated gas can potentially be applied on Fischer-Tropsch, acetic acid and oxo-synthesis process. Zhao Sun et al. [16] investigated the promoting mechanism of  $\text{Ca}_2\text{Fe}_2\text{O}_5$  for the inner-looping redox reaction and found that  $\text{Ca}_2\text{Fe}_2\text{O}_5$  facilitates  $\text{H}_2$  production. These studies collectively indicate that gasification efficiency and syngas yield were both enhanced by the introduction of OC. However, despite changing oxygen-rich air into solid OC, the gasification process itself remains largely unchanged, while the quality of produced syngas has seen some enhancement compared with traditional gasification, the original advantage of inherent separation of gas products [10] for chemical looping technology have not been fully realized. Later, the chemical looping hydrogen generation (CLHG) process was proposed with the aim of generating high purity hydrogen, especially with the inherent capture of high purity of  $\text{CO}_2$  [17–19]. However, the process requires that  $\text{Fe}_2\text{O}_3$  OC be reduced to Fe or  $\text{FeO}$  in the fuel reactor, as only Fe/ $\text{FeO}$  can be oxidized by steam to produce hydrogen [20]. While in practical terms,  $\text{Fe}_3\text{O}_4$  always exhibit poor reactivity to carbonaceous fuel, leading to issues such as serious carbon deposit (gaseous fuel), partial oxidation of fuel and low carbon conversion rate [21–23], these will hinder the capture of  $\text{CO}_2$ , furthermore, the unreacted carbon will influence the purity of hydrogen in the subsequent reactor. As a result, achieving the goals of the CLHG process is quite challenging.

Based on these situations, a new modified chemical looping gasification process, which we called chemical looping partial oxidation and hydrogen generation (CLPH) process, was proposed, and the schematic of CLPH was shown in Fig. 1. CLPH process consists of two reactors: partial oxidation reactor ( $\text{P}_{\text{oxR}}$ ) and steam reactor (SR). In  $\text{P}_{\text{oxR}}$ , solid fuel is partially oxidized to produce CO-rich gas by OC. Subsequently, the reduced OC reacts with steam in SR to generate high purity of hydrogen while simultaneously regenerating the OC. This results in the inherently separated production of syngas. Contrasted to CLHG process, the CLPH requires the partial oxidation of the fuel in  $\text{P}_{\text{oxR}}$ . Thus, the requirements for OC in the CLPH process are different from those in other processes. The OC utilized in CLPH process must exhibit excellent solid-solid reactivity and relatively low reactivity (or even inertness) with syngas. Jinzhi Zhang et al. [24] comprehensively investigated the chemical looping partial oxidation of carbon to find a suitable oxygen carrier that has a good reactivity and high CO selectivity for the reactions with carbon, their work revealed that  $\text{CaFe}_2\text{O}_4$  and  $\text{Ca}_2\text{Fe}_2\text{O}_5$  have a fast reaction rate, high CO selectivity and good regeneration performance. In addition, Ranjani Siriwardane et al. [25–27] comprehensively investigated the redox performance, kinetic analysis and reaction mechanism of  $\text{CaFe}_2\text{O}_4$  in chemical looping gasification process.

Table 1

Proximate and ultimate analyses of pinewood char.

Sample	Proximate analysis (wt%, d)			Ultimate analysis (wt%, daf)			
	A	V	FC	C	H	O*	N
Pinewood	8.77	0.39	90.84	90.3	2.47	6.56	0.55
				0.12			

d: dry basis; daf: dry ash-free basis; \*by difference

Jing Chen et al. [28] compared the performance of  $\text{MFe}_2\text{O}_4$ s ( $\text{M}=\text{Cu}, \text{Ba}, \text{Ni}, \text{Co}$ ) in the chemical looping reforming of char, and found that  $\text{BaFe}_2\text{O}_4$  has a higher reactivity in solid-solid reaction but a lower reactivity with pyrolysis gas. Jingchun Yan et al. [29] investigated the behaviors of  $\text{BaFe}_2\text{O}_4$  in the biomass chemical looping gasification process and the same results as that of Jing Chen et al. were obtained. Many studies have indicated that  $\text{CaFe}_2\text{O}_4$  and  $\text{BaFe}_2\text{O}_4$  demonstrate superior reactivity in solid-solid reaction while displaying limited reactivity with syngas. Therefore, these two OCs may be suitable for meeting the requirements of CLPH process.

The CLPH process, which combines two carbon-neutral processes (biomass utilization and hydrogen generation) together, has shown an obvious environment significance. Besides that, the generation of inherently separated syngas can significantly broaden its application range by artificial adjustment of the  $\text{CO}/\text{H}_2$  ratio for various chemical engineering processes. The CLPH process can easily generate high purity  $\text{H}_2$  with some miniaturized instruments, potentially avoiding issues associated with  $\text{H}_2$  transportation. This characteristic aligns well with the distributed and random nature of biomass. This objective of this study is to assess the feasibility of the proposed CLPH process and provide fundamental support for subsequent research on CLPH process. To achieve this, four ferrite OCs ( $\text{NiFe}_2\text{O}_4$ ,  $\text{CoFe}_2\text{O}_4$ ,  $\text{CaFe}_2\text{O}_4$  and  $\text{BaFe}_2\text{O}_4$ ) were employed in the proposed CLPH process to convert biomass char into inherently separated syngas. Comprehensively investigations were conducted, including thermodynamic simulations, fixed-bed experiments, cycle performance assessments, and DFT calculations of these OC in CLPH process.

## 2. Experimental Section

### 2.1. Materials preparation

Pinewood, which has a low content of ash, sulfur and nitrogen, was chosen as carbon feedstock, and pinewood char was made to avoid the effects of volatile matter. The ultimate and proximate analyses of pinewood char are given in Table 1.

$\text{MFe}_2\text{O}_4$  ( $\text{M}=\text{Ni}, \text{Co}, \text{Ca}, \text{Ba}$ ) was synthesized by a modified sol-gel method. Stoichiometric amounts of nitrates were dissolved in deionized water at  $50^\circ\text{C}$ , citric acid was then added as a complexing agent to enhance bonding [24], and aqueous ammonia was introduced to adjust the pH to 7.0. The mixture was stirred at  $80^\circ\text{C}$  for 6 h to evaporate most of the water, resulting in sol-gel state. The sol-gel was subsequently dried at  $105^\circ\text{C}$  for 12 h, preheated at  $450^\circ\text{C}$  for 2 h, and calcination at  $950^\circ\text{C}$  for 4 h. Finally, fresh  $\text{MFe}_2\text{O}_4$  was obtained by grinding and sieving the calcined sample to  $50\text{--}100 \mu\text{m}$ .

### 2.2. Thermodynamic simulation

The thermodynamic data used in the modified Ellingham diagram was obtained from FactSage 7.3 software. While thermodynamic simulation doesn't account for kinetic constraints and therefore has great limitations [30], it is capable of providing thermodynamic parameters and insights into the evolution behaviors of metal ferrites, all of these can give technical guidance for the selection of oxygen carriers [31,32].

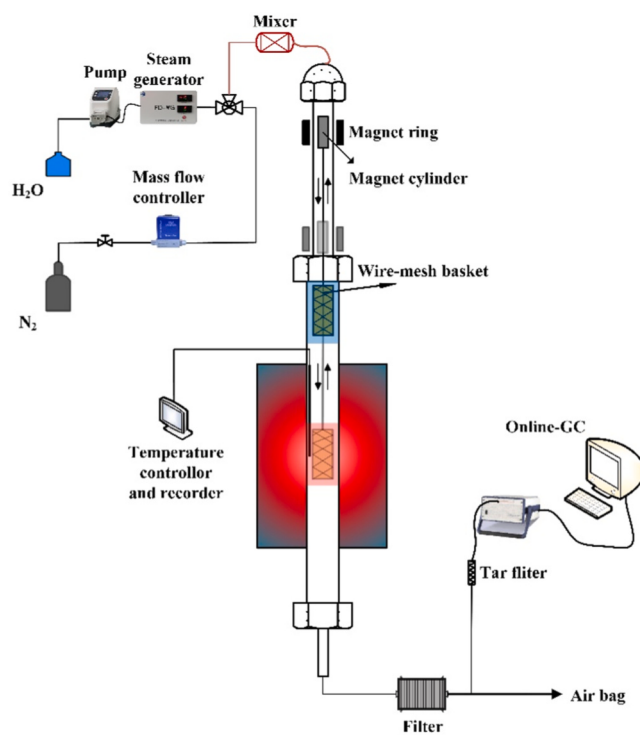


Fig. 2. The schematic diagram of the experimental apparatus.

**Table 2**  
Experimental procedure in a cycle.

No.	Section	Temperature (°C)	Time (min)	Gas flow rate (mL/min)
1	Partial oxidation	900	60	N <sub>2</sub> : 400
2	Steam oxidation	800	40	N <sub>2</sub> : 400; H <sub>2</sub> O(l): 9.8 mL/h

### 2.3. Fixed bed experiments

The chemical looping experiments were conducted in a fixed bed reactor, the schematic of the reactor was shown in Fig. 2. This reactor consisted of a control system, a fixed-bed reaction system and an off-gas treatment system. For each run, 0.1 g of biomass char with a certain mass of oxygen carrier was loaded in a wire-mesh basket, and the ratio of C in char to available O in OC was set to 1:2 according to the thermodynamic simulation in **Supplement**. The basket was initially put at the cooling zone, once the pre-set temperature was obtained, it was transported to the reaction zone by using the magnet ring. After reaction, the basket was returned the cooling zone and cooled under a N<sub>2</sub> atmosphere. The experimental procedures for each cycle were shown in Table 2. All experiments were repeated three times to make sure the results are reliable.

### 2.4. Characteristics

The composition of outlet gas was analyzed by a micro-GC (Agilent 3000) with two channels, where channel A was used to separate H<sub>2</sub>, O<sub>2</sub>, N<sub>2</sub>, CH<sub>4</sub> and CO, channel B was used to separate CO<sub>2</sub> and C<sub>2</sub>-C<sub>4</sub>, the relative standard deviation (RSD) for standard gas was below 0.5%. The proximate and ultimate analyses were conducted according to the Chinese National Standards of GB/T 212–2008 and GB 476–91, respectively. The phase composition of OC was detected by an X-ray diffraction analyzer (XRD, D8 Advance, Bruker, Germany), where a Cu K $\alpha$  radiation ( $\lambda = 1.54056 \text{ \AA}$ ), tube current of 15 mA, accelerating voltage of 30 kV

**Table 3**  
Main reactions during the CLPH process.

Partial oxidation reactor	Steam reactor
$2\text{MeO}_x \rightleftharpoons 2\text{MeO}_{x-1} + \text{O}_2$	(1) $2\text{H}_2\text{O} \rightleftharpoons 2\text{H}_2 + \text{O}_2$
$2\text{C} + \text{O}_2 \rightleftharpoons 2\text{CO}$	(2) $\text{MeO}_{x-1} + \text{O}_2 \rightleftharpoons \text{MeO}_x$
$2\text{CO} + \text{O}_2 \rightleftharpoons 2\text{CO}_2$	(3)

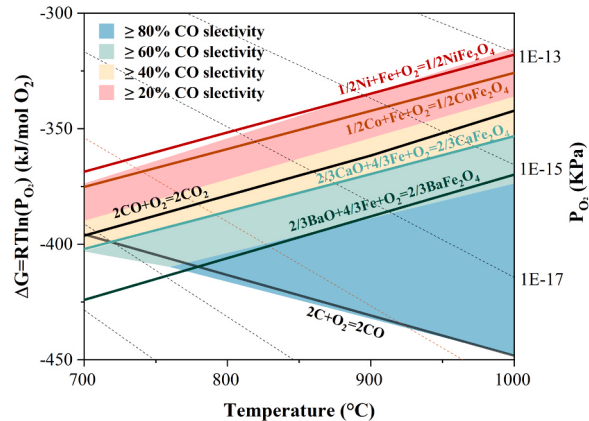


Fig. 3. Ellingham diagram for the partial oxidation reactions of carbon.

and scan rate of 4 °/min with 20 in the range of 10 ° and 80 ° were used. The H<sub>2</sub>-TPR was carried out by a dynamic adsorption apparatus (DAS-7010, Huasi, China), where 30 mg of sample, a flow rate of 30 mL/min H<sub>2</sub>/N<sub>2</sub> with 5% of hydrogen, a temperature range of 200–950 °C with a heating rate of 10 °C/min were used. The surface morphology of the OC was recorded by a JEOL field emission scanning electron microscope (FESEM, JSM-7001 F). The surface properties of fresh and used OCs were tested by an XPS spectrometer (Thermo Scientific K-Alpha), where Al K $\alpha$  monochromatic X-ray source, a spot size of 400 μm, filament current of 6 mA, base pressure of  $3 \times 10^{-5}$  pa were used.

### 2.5. Computational methods

The energy of lattice O and reaction pathways of BaFe<sub>2</sub>O<sub>4</sub> with C and CO were calculated by the Vienna Ab Initio Simulation Package (VASP) [33,34]. The projector augmented wave pseudopotentials were used to describe the interaction of electron-ion. A spin-polarized Generalized Gradient Approximation-Perdew Burke Ernzerhof (GGA-PBE) [35] was used to represent exchange-correlation function. The cut-off energy was set to 480 eV, while a 5 × 5 × 2 k-points was adopted for the primitive cell. Owing to the strong electron correlation of transition metals, LDA+U scheme was used, U<sub>eff</sub> of 4.2 eV, 2.4 eV and 1.2 eV was adopted for Fe 3d, Co 3d and Ni 3d electrons [36–38]. For the calculation of transition state, the method of climbing-image nudge elastic band (CINEB) was used [39].

## 3. Results and discussion

### 3.1. Preliminary selection of OC

The reaction of CLPH process is concluded in Table 3. The performance of oxygen carrier is the key to the CLPH process. A high syngas productivity, high CO selectivity, good reactivity and redox stability are desired for the oxygen carrier. From a thermodynamic perspective, OC can be seen as an oxygen resource during the partial oxidation of char (Eqs. 1). Thus, the redox pair of MeO<sub>x</sub>/MeO<sub>x-1</sub>, which has a high P<sub>O2</sub>, may result in the over oxidation of carbon and CO (Eqs. 3), leading to the generation of CO<sub>2</sub> rather than CO-rich gas. Conversely, a low P<sub>O2</sub> can lead to a better activity of partial oxidation (Eqs. 2) [40]. So, the

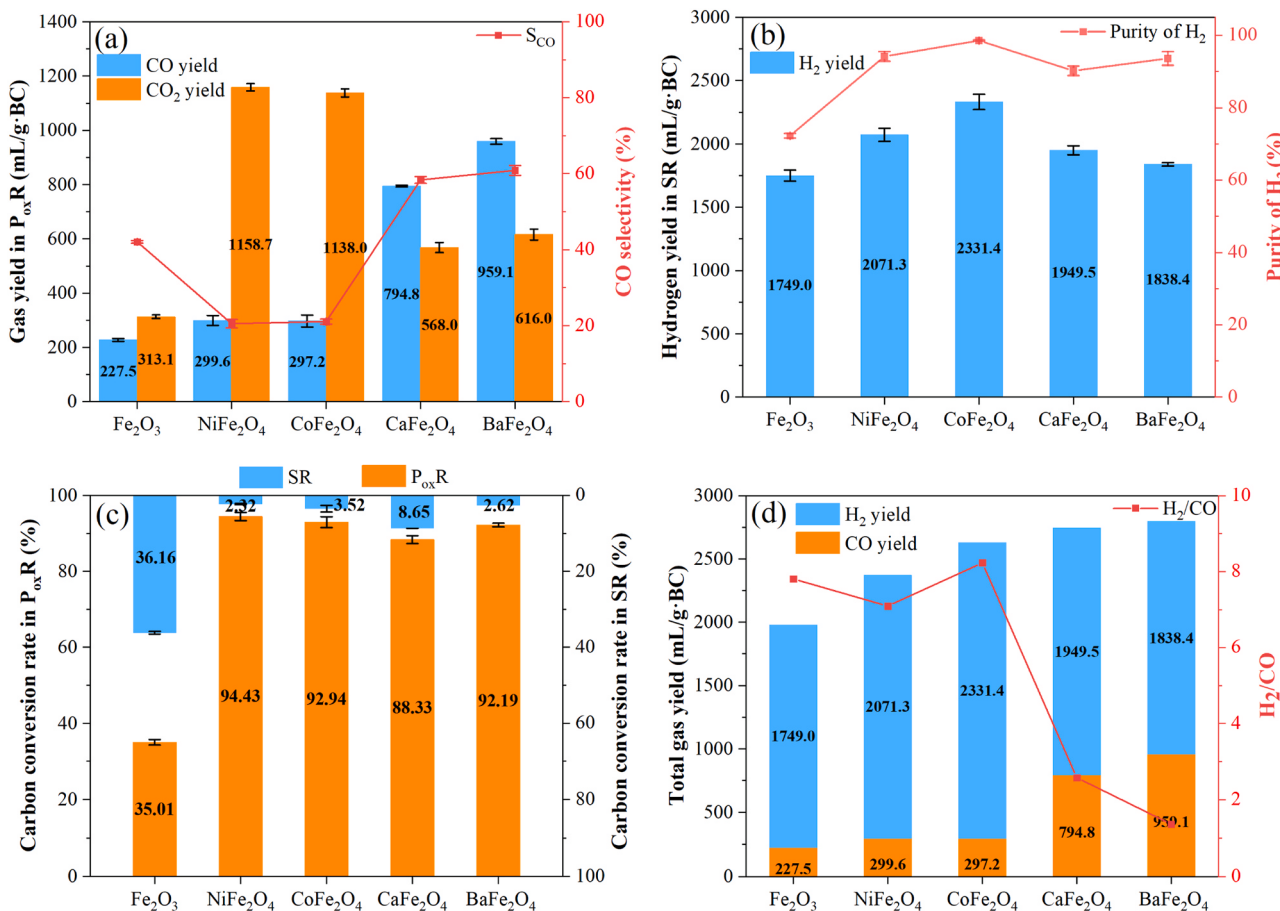


**Fig. 4.** (a) Gas yield in  $P_{ox}R$ , (b) hydrogen yield in SR, (c) carbon conversion rate in  $P_{ox}R$  and SR, (d) total gas yield of the selected OCs.

selection of appropriate OC was essential to the proposed CLPH process. The modified Ellingham diagram, depicting the relationship among CO selectivity, temperature, oxygen pressure and standard Gibbs free energy ( $\Delta G$ ), was shown in Fig. 3. The thermodynamic parameters were obtained from FactSage 7.3, and the thermodynamic parameters of BaFe<sub>2</sub>O<sub>4</sub> were sourced from the reference [41], and 1 mol of oxygen was taken as a reference [24,42]. The  $\Delta G$  lines of different oxygen carriers in this modified Ellingham diagram can reflect the potential reduction and oxidation activities of these materials [40,43]. As shown in Fig. 3, equilibrium  $P_{O_2}$  line of CO/CO<sub>2</sub> pair serve as the boundary between partial oxidation and over oxidation, so NiFe<sub>2</sub>O<sub>4</sub> and CoFe<sub>2</sub>O<sub>4</sub>, located above the CO/CO<sub>2</sub> line, are preferred for oxidizing CO to CO<sub>2</sub>. In contrast, CaFe<sub>2</sub>O<sub>4</sub> and BaFe<sub>2</sub>O<sub>4</sub>, located below the CO/CO<sub>2</sub> line, are favored for oxidizing carbon to CO, and what's more, CO cannot be easily oxidized to CO<sub>2</sub> [44]. Therefore, theoretically, the CO selectivity of these four materials follows the order of BaFe<sub>2</sub>O<sub>4</sub> > CaFe<sub>2</sub>O<sub>4</sub> > CoFe<sub>2</sub>O<sub>4</sub> > NiFe<sub>2</sub>O<sub>4</sub>.

### 3.2. Fixed bed experiments

#### 3.2.1. Redox performance

The redox performances of the selected OCs were shown in Fig. 4. It could be seen that all the OCs exhibit outstanding activity for solid-solid reaction. Among them, NiFe<sub>2</sub>O<sub>4</sub>, CoFe<sub>2</sub>O<sub>4</sub> and BaFe<sub>2</sub>O<sub>4</sub> has a superior activity for solid-solid reaction, which can get an  $X_c$  of 94.43%, 92.94% and 92.19%, respectively. Besides that, based on CO selectivity (Fig. 4a), NiFe<sub>2</sub>O<sub>4</sub> and CoFe<sub>2</sub>O<sub>4</sub> exhibit approximately 20% CO selectivity, signifying that these two OCs are more suitable for chemical looping combustion (CLC) rather than CLPH. In contrast, CaFe<sub>2</sub>O<sub>4</sub> and BaFe<sub>2</sub>O<sub>4</sub> both exhibit a high CO selectivity and can generate syngas with a high

concentration of CO, thus these two OCs both can be candidate for CLPH process. However, the  $X_c$  for CaFe<sub>2</sub>O<sub>4</sub> is 88.33%, indicating a poorer reactivity compared to that of the BaFe<sub>2</sub>O<sub>4</sub> (92.19%). Consequently, the CO production of CaFe<sub>2</sub>O<sub>4</sub> (794.8 mL/g·Biomass Char) was lower than that of BaFe<sub>2</sub>O<sub>4</sub> (959.1 mL/g·BC), despite their similar CO selectivity. The results of CO selectivity of these four candidate OCs are well consistent with that of Ellingham diagram.

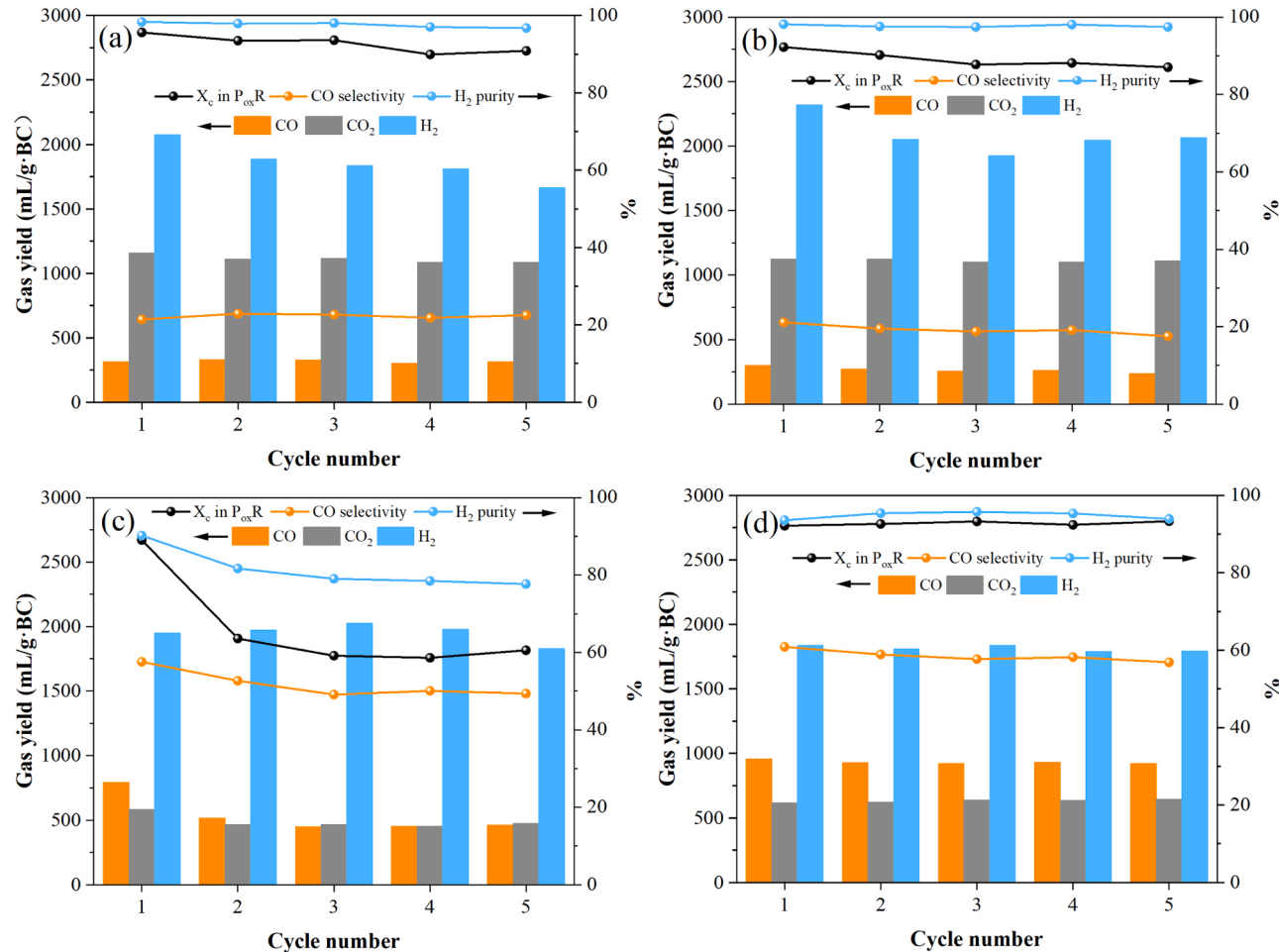
For H<sub>2</sub> production in Fig. 4b, CoFe<sub>2</sub>O<sub>4</sub> exhibits superior hydrogen generation capability, producing a hydrogen yield of 2331.44 mL/g·biomass char, while CaFe<sub>2</sub>O<sub>4</sub>, NiFe<sub>2</sub>O<sub>4</sub> and BaFe<sub>2</sub>O<sub>4</sub> can generate a hydrogen yield of 1949.51 mL/g·BC, 2071.3 mL/g·BC and 1838.4 mL/g·BC, respectively. For the quality of the generated hydrogen, CoFe<sub>2</sub>O<sub>4</sub>, NiFe<sub>2</sub>O<sub>4</sub> and BaFe<sub>2</sub>O<sub>4</sub> all can get a high quality of H<sub>2</sub> with a purity of 98.6%, 94.2% and 93.6%, respectively. While, CaFe<sub>2</sub>O<sub>4</sub> can get a 90.8% purity of H<sub>2</sub> which is attributed to the low reactivity, the low  $X_c$  in P<sub>ox</sub>R means that unreacted carbon is kept and will enter SR and react with steam, this will form CO and make the hydrogen impure. Thus, the  $X_c$  in P<sub>ox</sub>R /SR (Fig. 4c) can serve as an indicator of the hydrogen purity, and the higher carbon conversion rate in P<sub>ox</sub>R (a high  $X_c$  in P<sub>ox</sub>R / a low  $X_c$  in SR), the higher purity of hydrogen can be generated in SR.

The total gas yield of these OCs is shown in Fig. 4d. As we can see, the syngas generation of CoFe<sub>2</sub>O<sub>4</sub>, CaFe<sub>2</sub>O<sub>4</sub> and BaFe<sub>2</sub>O<sub>4</sub> was higher than that of NiFe<sub>2</sub>O<sub>4</sub>. While NiFe<sub>2</sub>O<sub>4</sub> and CoFe<sub>2</sub>O<sub>4</sub> both show a high selectivity of CO<sub>2</sub> and a high purity of generated hydrogen, CoFe<sub>2</sub>O<sub>4</sub> has a better performance on hydrogen generation than NiFe<sub>2</sub>O<sub>4</sub>, this finding aligns with Shiyi Chen et al. [17] which also found that NiFe<sub>2</sub>O<sub>4</sub> has a limited hydrogen generation capacity. Therefore, CoFe<sub>2</sub>O<sub>4</sub> is suitable for the CLHG process. For CaFe<sub>2</sub>O<sub>4</sub> and BaFe<sub>2</sub>O<sub>4</sub>, both of them have a high selectivity for CO, and can generate more syngas than NiFe<sub>2</sub>O<sub>4</sub> and CoFe<sub>2</sub>O<sub>4</sub>. In addition, BaFe<sub>2</sub>O<sub>4</sub> exhibit better solid-solid reactivity,

**Table 4**

Transformation behaviors of OCs in different reactors.

P <sub>ox</sub> R	SR	AR	
NiFe <sub>2</sub> O <sub>4</sub>	NiFe <sub>2</sub> O <sub>4</sub> → Char Fe <sub>3</sub> O <sub>4</sub> + FeO + Ni <sub>3</sub> Fe Fe <sub>3</sub> O <sub>4</sub> → Char FeO FeO + Ni <sub>3</sub> Fe → Char NiFe	NiFe → Steam Fe <sub>3</sub> O <sub>4</sub> + Ni FeO → Steam Fe <sub>3</sub> O <sub>4</sub>	Fe <sub>3</sub> O <sub>4</sub> + Ni → Air NiFe <sub>2</sub> O <sub>4</sub>
CoFe <sub>2</sub> O <sub>4</sub>	CoFe <sub>2</sub> O <sub>4</sub> → Char Fe <sub>3</sub> O <sub>4</sub> + FeO + Co Fe <sub>3</sub> O <sub>4</sub> → Char FeO FeO + Co → Char CoFe	CoFe → Steam Fe <sub>3</sub> O <sub>4</sub> + CoO	Fe <sub>3</sub> O <sub>4</sub> + CoO → Air CoFe <sub>2</sub> O <sub>4</sub>
CaFe <sub>2</sub> O <sub>4</sub>	CaFe <sub>2</sub> O <sub>4</sub> → Char Ca <sub>2</sub> Fe <sub>2</sub> O <sub>5</sub> + FeO Ca <sub>2</sub> Fe <sub>2</sub> O <sub>5</sub> → Char Ca <sub>2</sub> Fe <sub>2</sub> O <sub>5</sub> + CaO + FeOFeO → Char Fe	CaO + Fe → Steam Fe <sub>3</sub> O <sub>4</sub> + Ca <sub>2</sub> Fe <sub>2</sub> O <sub>5</sub>	Fe <sub>3</sub> O <sub>4</sub> + Ca <sub>2</sub> Fe <sub>2</sub> O <sub>5</sub> → Air CaFe <sub>2</sub> O <sub>4</sub>
BaFe <sub>2</sub> O <sub>4</sub>	BaFe <sub>2</sub> O <sub>4</sub> → Char Ba <sub>2</sub> Fe <sub>2</sub> O <sub>5</sub> + FeBa <sub>2</sub> Fe <sub>2</sub> O <sub>5</sub> → Char Ba <sub>3</sub> Fe <sub>2</sub> O <sub>6</sub> + Fe	Ba <sub>2</sub> Fe <sub>2</sub> O <sub>5</sub> + Fe → Steam BaFe <sub>2</sub> O <sub>4</sub> Ba <sub>3</sub> Fe <sub>2</sub> O <sub>6</sub> + Fe → Steam BaFe <sub>2</sub> O <sub>4</sub>	No need

**Fig. 5.** Cycle performance of the selected OCs. (a) NiFe<sub>2</sub>O<sub>4</sub>, (b) CoFe<sub>2</sub>O<sub>4</sub>, (c) CaFe<sub>2</sub>O<sub>4</sub>, (d) BaFe<sub>2</sub>O<sub>4</sub>.

yielding approximately 150 mL/g·BC more CO than that of the CaFe<sub>2</sub>O<sub>4</sub> in P<sub>ox</sub>R, while CaFe<sub>2</sub>O<sub>4</sub> can generate 100 mL/g·BC more H<sub>2</sub> than that of BaFe<sub>2</sub>O<sub>4</sub> in SR due to the gasification reaction of unreacted carbon in P<sub>ox</sub>R. Consequently, the fixed bed experiments results show that both CaFe<sub>2</sub>O<sub>4</sub> and BaFe<sub>2</sub>O<sub>4</sub> are suitable for the CLPH process, but further comparisons experiments are necessary.

### 3.2.2. Transformation behaviors

The transformation behaviors of OCs during CLPH process were comprehensively investigated by XRD, and the results and discussions were shown in **Supplement**. The detailed transformation behaviors were summarized in **Table 4**. From **Table 4**, it is evident that the regeneration of NiFe<sub>2</sub>O<sub>4</sub>, CoFe<sub>2</sub>O<sub>4</sub> and CaFe<sub>2</sub>O<sub>4</sub> cannot be completed in SR, thus another reactor, i.e., the AR is required. In contrast, BaFe<sub>2</sub>O<sub>4</sub>

can be easily regenerated by steam in SR, indicating that BaFe<sub>2</sub>O<sub>4</sub> can greatly reduce the equipment investment and operational risk during the CLPH process. Moreover, based on the behaviors of CoFe<sub>2</sub>O<sub>4</sub> in SR, it can be inferred that the excellent hydrogen generation property exhibited by CoFe<sub>2</sub>O<sub>4</sub> is due to the fact that Co can be oxidized by steam and generate hydrogen, while Ni cannot.

### 3.2.3. Cycle experiments

In addition to the redox performance of OC, the cycle performance was also essential for the process. Therefore, cycle experiments of the selected OC were conducted, and the results were shown in **Fig. 5**. For NiFe<sub>2</sub>O<sub>4</sub> and CoFe<sub>2</sub>O<sub>4</sub>, both of them have a good cycle performance on X<sub>c</sub>, CO selectivity and gas yield in P<sub>ox</sub>R, only a slight decline in hydrogen yield (SR) was observed (from 2075.8 to 1665.8 mL/g·BC for NiFe<sub>2</sub>O<sub>4</sub>

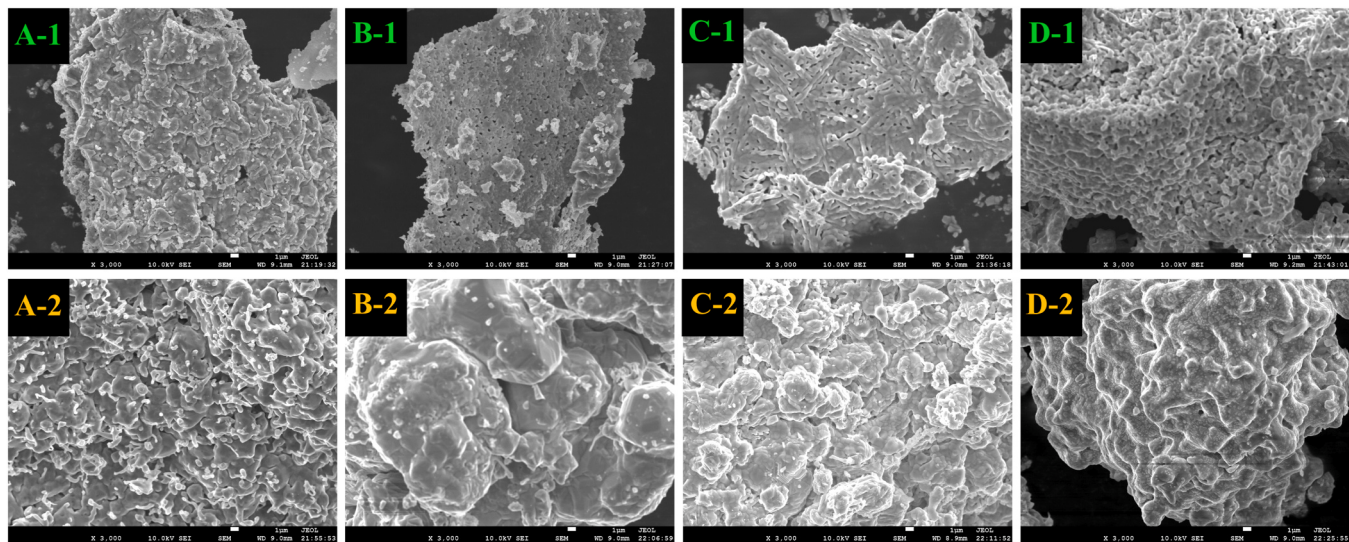


**Fig. 6.** Surface morphology of the (1) fresh OC and (2) 5-cycled OC. A: NiFe<sub>2</sub>O<sub>4</sub>, B: CoFe<sub>2</sub>O<sub>4</sub>, C: CaFe<sub>2</sub>O<sub>4</sub>, D: BaFe<sub>2</sub>O<sub>4</sub>.

and from 2331.4 mL/g-BC to 2095.1 mL/g-BC). And both of them can get a ≥ 95% purity of hydrogen over 5 cycles. Besides that, the hydrogen yield of CoFe<sub>2</sub>O<sub>4</sub> (2331.4–2095.1 mL/g-BC) was approximately 300 mL/g-BC higher than that of the NiFe<sub>2</sub>O<sub>4</sub> (1665.8–2075.8 mL/g-BC). Therefore, according to the low CO selectivity and good performance in hydrogen production, CoFe<sub>2</sub>O<sub>4</sub> is not suitable for CLPH process, but it can be an ideal candidate for CLHG process.

For CaFe<sub>2</sub>O<sub>4</sub> in Fig. 5c, a rapid deactivation was observed after the first cycle. Fresh CaFe<sub>2</sub>O<sub>4</sub> initially showed an excellent performance not only in CO selectivity but also in hydrogen generation. However, after the first cycle, the solid-solid reactivity of CaFe<sub>2</sub>O<sub>4</sub> dramatically decreased. X<sub>c</sub> decreased from 89.1% to 63.6% after the first cycle, and then stabilized at around 60%, CO selectivity stabilized at around 50%, and the purity of hydrogen in SR decreased from 90.2% to 81.7% and then stabilized at around 78%. For BaFe<sub>2</sub>O<sub>4</sub> in Fig. 5d, BaFe<sub>2</sub>O<sub>4</sub> exhibits a wonderful cycle performance and can get an X<sub>c</sub> of around 93% over 5 cycles, owing to the excellent reactivity and CO selectivity of BaFe<sub>2</sub>O<sub>4</sub>, it can generate around 900 mL/g-BC of CO with a CO selectivity of 58% over 5 cycles. In SR, CaFe<sub>2</sub>O<sub>4</sub> can generate around 1900 mL/g-BC of H<sub>2</sub> which is higher than that of BaFe<sub>2</sub>O<sub>4</sub> (around 1800 mL/g-BC), but owing to the bad stability of CaFe<sub>2</sub>O<sub>4</sub>, the H<sub>2</sub> purity of CaFe<sub>2</sub>O<sub>4</sub> can only reach around 83% after the first cycle, whereas the H<sub>2</sub> purity of BaFe<sub>2</sub>O<sub>4</sub> can

reach around 94% even after 5 cycles. Therefore, based on these results, CaFe<sub>2</sub>O<sub>4</sub> cannot act as an appropriate OC for CLPH process due to its bad performance in cycle experiments. In summary, BaFe<sub>2</sub>O<sub>4</sub> can achieve an excellent cycle performance, high carbon conversion rate (93%), high purity of hydrogen (94%) and an approximately 60% CO selectivity over five cycles. Additionally, the regeneration of BaFe<sub>2</sub>O<sub>4</sub> can be completed by steam in the SR, eliminating the need for further oxidation by air, this feature will largely lower the cost of equipment and operation, thus BaFe<sub>2</sub>O<sub>4</sub> is expected to be the ideal OC for the CLPH process.

What's more, the 10 cycle experiments of BaFe<sub>2</sub>O<sub>4</sub> was conducted, and the results was shown in Fig. S 3. It can be seen that BaFe<sub>2</sub>O<sub>4</sub> exhibit good cycle performance in 10 cycles, only a little decline on the carbon conversion rate, hydrogen purity and hydrogen yield were observed, this decline is largely owing to the loss of the OC during the operational process.

### 3.3. Characterization of the OCs

#### 3.3.1. Surface characters

The surface morphology of fresh and cycled OCs is shown in Fig. 6. Fresh NiFe<sub>2</sub>O<sub>4</sub> and CoFe<sub>2</sub>O<sub>4</sub> show a smooth and uniformly close-contacted arrangement of small, plate-shape particles. While after 5

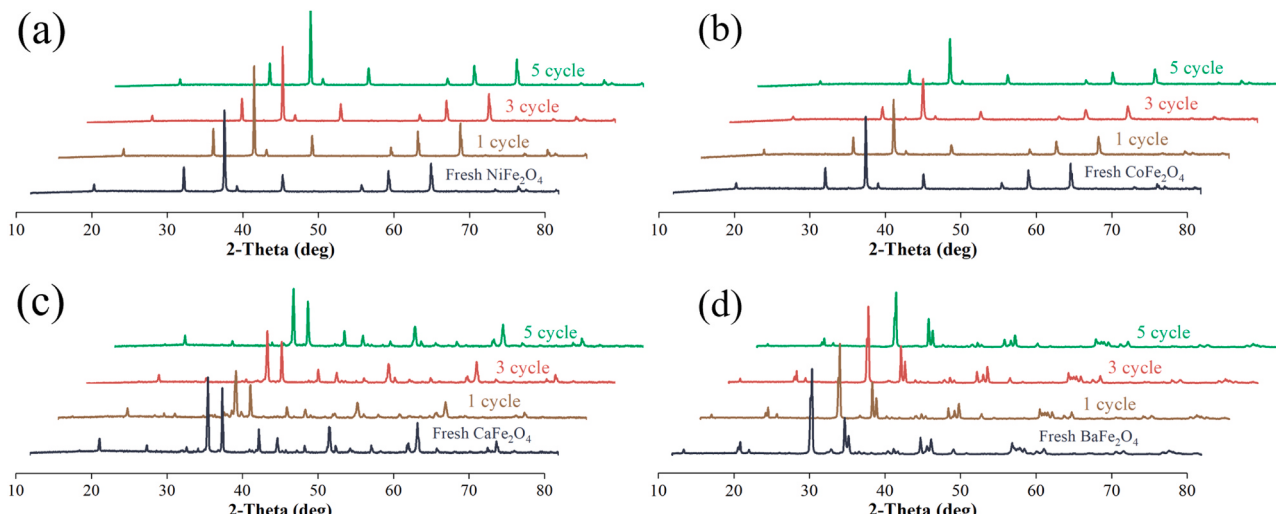


**Fig. 7.** XRD spectra of the fresh and cycled OC. (a) NiFe<sub>2</sub>O<sub>4</sub>, (b) CoFe<sub>2</sub>O<sub>4</sub>, (c) CaFe<sub>2</sub>O<sub>4</sub>, (d) BaFe<sub>2</sub>O<sub>4</sub>.

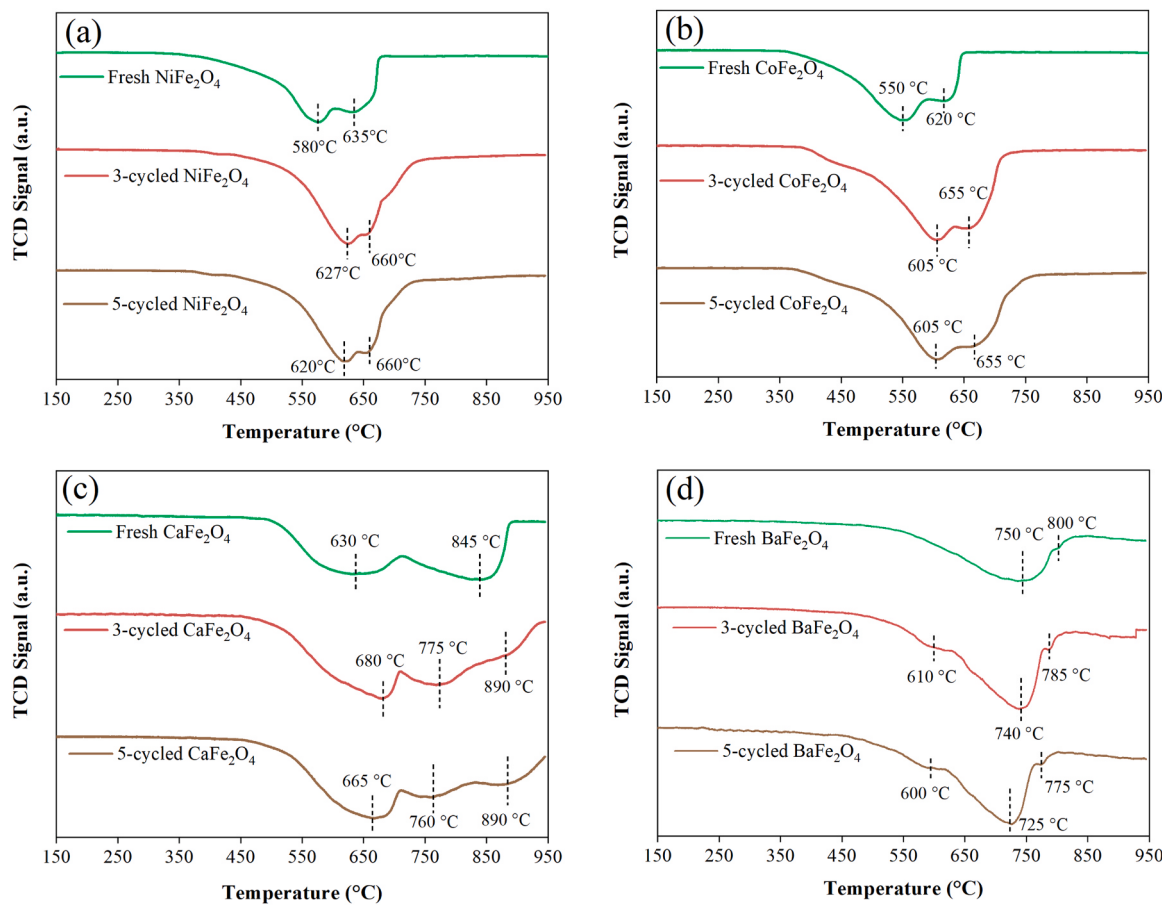


**Fig. 8.** H<sub>2</sub>-TPR of the fresh and cycled OC. (a) NiFe<sub>2</sub>O<sub>4</sub>, (b) CoFe<sub>2</sub>O<sub>4</sub>, (c) CaFe<sub>2</sub>O<sub>4</sub>, (d) BaFe<sub>2</sub>O<sub>4</sub>.

redox cycles, the surface of NiFe<sub>2</sub>O<sub>4</sub> turned to uneven and rough, with some aggregation observed. And for CoFe<sub>2</sub>O<sub>4</sub>, the compact plate-shaped structure was destroyed, big grains were generated and serious aggregations were observed. The sintering of OC leads to the decline of the hydrogen yield for NiFe<sub>2</sub>O<sub>4</sub> and CoFe<sub>2</sub>O<sub>4</sub>, while it seems that the sintering of OC has little influence on OC performance in P<sub>oxR</sub>. For fresh CaFe<sub>2</sub>O<sub>4</sub>, a poor porosity, instant-noodle shape and little aggregation were observed on its surface, which was owing to a high calcination temperature. While after five redox cycles, the original structure was completely destroyed and a serious aggregation was observed. For fresh BaFe<sub>2</sub>O<sub>4</sub>, it was a compact of small fragments with a good porosity, but after 5 redox cycles, the porosity disappeared and the small fragments merged together and form a whole. In conclusion, the surface morphology has little influence on the OC performance in P<sub>oxR</sub> (Fig. 5), only CaFe<sub>2</sub>O<sub>4</sub> shows obvious deactivation. While for the hydrogen generation, the sintering of the OC may contribute to the decline of the hydrogen generation for NiFe<sub>2</sub>O<sub>4</sub> and CoFe<sub>2</sub>O<sub>4</sub>, whereas BaFe<sub>2</sub>O<sub>4</sub> doesn't exhibit a significant impact, this difference may be attributed to the different oxidation pathway of BaFe<sub>2</sub>O<sub>4</sub> and Ni/CoFe<sub>2</sub>O<sub>4</sub> (Table 4).

### 3.3.2. XRD spectra

The XRD spectra of fresh, 1-cycled, 3-cycled and 5-cycled OC were shown in Fig. 7. In comparison with fresh OC, the XRD pattern of cycled samples showed no significant variation, demonstrating that all the selected OCs could be effectively regenerated after 5 cycles of redox reaction in terms of changes in phase. No clear clue indicated the existence of interactions between OC and biomass ash, this was largely contributed to the low ash content of the pinewood biomass.

### 3.3.3. H<sub>2</sub>-TPR experiments

From the XRD spectra of the cycled OC, it can be seen that the phase didn't show significant changes after 5 redox cycles. Therefore, the variation in performance during the redox cycle experiments wasn't owing to the phase transition. Consequently, H<sub>2</sub>-TPR experiments which reflected the redox reactivity of OCs were conducted, the results of fresh and cycled OC were shown in Fig. 8. For fresh NiFe<sub>2</sub>O<sub>4</sub>, the maximum peak emerged at 580 °C and accompanied by a satellite peak at 635 °C, the peak at 580 °C was deemed as an overlapped peak of reduction process of NiFe<sub>2</sub>O<sub>4</sub> → Ni + Fe<sub>3</sub>O<sub>4</sub> → Ni + FeO, and the peak at 635 °C was deemed as the reduction process of FeO → Fe [28]. While after the cycle experiments, the two peaks both moved to the high-temperature range and approached each other, these indicated a little deactivation of the redox reactivity for NiFe<sub>2</sub>O<sub>4</sub>. Similar to NiFe<sub>2</sub>O<sub>4</sub>, the H<sub>2</sub>-TPR of CoFe<sub>2</sub>O<sub>4</sub> exhibits a similar behavior during cycles. From the SEM and cycle experiments, it can be concluded that the sintering of the OC may contribute to the decline of the hydrogen generation for NiFe<sub>2</sub>O<sub>4</sub> and CoFe<sub>2</sub>O<sub>4</sub>. And the H<sub>2</sub>-TPR peaks show a distinct shift to the high temperature, demonstrating alterations on the OC surface [45] during the cycle experiments, it is possible that NiO/CoO is generated on the surface of the OC during the cycling process, leading to an exchange of the active sites on the surface, and the formation of NiO/CoO also hindered the hydrogen generation capacity.

For fresh CaFe<sub>2</sub>O<sub>4</sub>, two distinct peaks were observed at 630 °C and 845 °C. Based on the transformation behaviors, these two peaks were considered to be the reduction process of CaFe<sub>2</sub>O<sub>4</sub> → Ca<sub>2</sub>Fe<sub>2</sub>O<sub>5</sub> + FeO and Ca<sub>2</sub>Fe<sub>2</sub>O<sub>5</sub> + FeO → CaO + Fe, respectively. But after the cycle experiments, the two peaks split into three peaks which emerged at 665 °C, 760 °C and 880 °C respectively, this phenomenon indicated that the structure of CaFe<sub>2</sub>O<sub>4</sub> has a major influence during the cycle experiments,

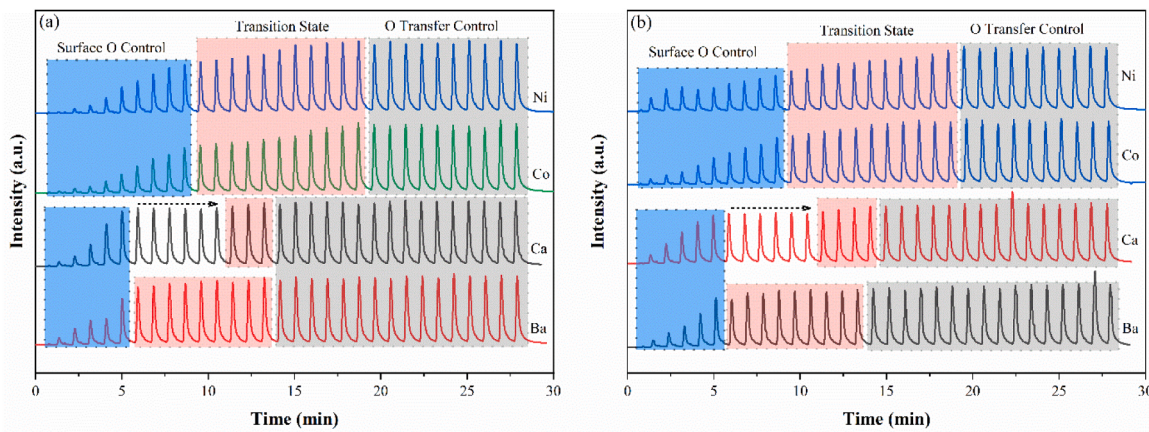


**Fig. 9.** H<sub>2</sub>-pulse experiments of the fresh and cycled OC. (a) Fresh OC, (b) 5-cycled OC.

even though there was little changes in phase were observed. The redox reactivity of CaFe<sub>2</sub>O<sub>4</sub> changed a lot according to the H<sub>2</sub>-TPR experiments, which results in a dramatical decrease in the redox performance after the first cycle. For BaFe<sub>2</sub>O<sub>4</sub>, a maximum peak at around 750 °C was observed, this peak was an aggregation of the peaks of BaFe<sub>2</sub>O<sub>4</sub> → Ba<sub>2</sub>Fe<sub>2</sub>O<sub>5</sub> + Fe → Ba<sub>3</sub>Fe<sub>2</sub>O<sub>6</sub> + Fe, and after the cycle experiments, unlike Ni/CoFe<sub>2</sub>O<sub>4</sub>, the temperature of maximum peak for BaFe<sub>2</sub>O<sub>4</sub> shifts to a lower range after the cycle, indicating an increase on redox property, which is well consistent with the cycle experiments results. This enhancement in redox property is probably due to the fact that the regeneration of BaFe<sub>2</sub>O<sub>4</sub> doesn't need an air reactor, and the reaction between reduced OC and steam will generate more active sites on the surface, while the reaction with air will induce severe sintering on the surface, therefore, NiFe<sub>2</sub>O<sub>4</sub>/CoFe<sub>2</sub>O<sub>4</sub> exhibit different performance. The results of Fig. 8 clearly demonstrate that the cycle performances of NiFe<sub>2</sub>O<sub>4</sub>, CoFe<sub>2</sub>O<sub>4</sub> and BaFe<sub>2</sub>O<sub>4</sub> are much better than that of the CaFe<sub>2</sub>O<sub>4</sub>, and these results are well consistent with that of cycle experiments.

### 3.3.4. H<sub>2</sub>-pulse experiments

Chemical looping process is a typical Mars-van Krevelen reaction [46]. During the CLPH process, carbon will firstly be oxide by the surface O of OC. Subsequently, the bulk O will transfer to the surface to replenish the oxygen vacancy and sustain the oxidation reaction. The lattice oxygen property of OC can be reflected through the H<sub>2</sub>-pulse experiments as shown in Fig. 9. It's clear that there are always three stages for the lattice oxygen during the reduction process of H<sub>2</sub>, the first stage is controlled by the surface O of OC, where the reduction of the surface oxygen occurs [47–50]. The subsequent transition stage is controlled by both surface O activity and O transfer capacity. The third is the O transfer control stage, where O transfer capacity is the rate-determining step. From Fig. 9, it's apparent that the surface O of Ca/BaFe<sub>2</sub>O<sub>4</sub> is lower than that of the Ni/CoFe<sub>2</sub>O<sub>4</sub>, which inducing the excellent CO selectivity of Ca/BaFe<sub>2</sub>O<sub>4</sub>. For the 5-cycled experiments, CoFe<sub>2</sub>O<sub>4</sub> and BaFe<sub>2</sub>O<sub>4</sub> exhibit no obvious change, whereas an obvious decline in the surface O of NiFe<sub>2</sub>O<sub>4</sub> and CaFe<sub>2</sub>O<sub>4</sub> are observed. Owing to the high oxygen activity of NiFe<sub>2</sub>O<sub>4</sub>, the decline of surface O doesn't influence the cycle performance of NiFe<sub>2</sub>O<sub>4</sub>, while it adversely affects the cycle performance of CaFe<sub>2</sub>O<sub>4</sub>. In addition, it's interesting that there is a flat stage for CaFe<sub>2</sub>O<sub>4</sub> between the Surface O Control stage and the Transition stage, this may due to the generation of another stable phase during the H<sub>2</sub>-reduction process, which could be the Ca<sub>2</sub>Fe<sub>2</sub>O<sub>5</sub> generated on the surface of OC.

### 3.3.5. XPS spectra

In order to further investigate the cause of CaFe<sub>2</sub>O<sub>4</sub> deactivation, XPS, an effective method to confirm the state of atoms on the surface of

OC [29], were conducted, the high-resolution XPS spectra of the Fe2p peaks for the fresh and 5-cycled OCs were shown in Fig. 10. The curve fitting of Fe2p spectra in Fig. 10 showed the presence of not only Fe<sup>3+</sup> but also Fe<sup>2+</sup> on the surface of OC [51,52]. The observation of Fe<sup>2+</sup> on the surface of fresh OC was largely attributed to the existence of oxygen vacancy [29,53]. In the crystal structure of MFe<sub>2</sub>O<sub>4</sub>, the central M<sup>2+</sup> ion can exert a drag force (G) on the surface O<sup>2-</sup> ion. However, due to the incomplete nature of the crystal structure on the surface, the surface O<sup>2-</sup> has a tendency to form oxygen vacancy (F). When the leaving force F exceeds the drag force G, oxygen vacancy are formed. This vacancy then disrupts the charge balance in the spinel structure, causing the valence electrons of Fe<sup>3+</sup> which is close to the O vacancy to decrease in order to maintain charge balance, resulting in the transformation of Fe<sup>3+</sup> to Fe<sup>2+</sup>. In the chemical looping partial oxidation of biomass char, the predominant reaction was solid-solid reaction. More oxygen vacancy on the surface of OC implies fewer lattice-oxygen directly contacted to char, thus inducing a better CO selectivity. The amount of Fe<sup>2+</sup> can reflect the quantity of oxygen vacancy on the surface, Consequently, the higher the content of Fe<sup>2+</sup> on the surface of OC, the better the CO selectivity of the OC. The proportion of Fe<sup>2+</sup> in fresh OCs were 32.30%, 32.71%, 46.62% and 54.91% for NiFe<sub>2</sub>O<sub>4</sub>, CoFe<sub>2</sub>O<sub>4</sub>, CaFe<sub>2</sub>O<sub>4</sub> and BaFe<sub>2</sub>O<sub>4</sub>, respectively. These results were well consistent with the CO selectivity results in fixed bed experiments. After 5 redox cycles, only a little increase in the proportions of Fe<sup>2+</sup> was observed for NiFe<sub>2</sub>O<sub>4</sub>, CoFe<sub>2</sub>O<sub>4</sub> and BaFe<sub>2</sub>O<sub>4</sub>, but for CaFe<sub>2</sub>O<sub>4</sub>, the proportion of Fe<sup>2+</sup> increased significantly after 5 cycles, this indicated that CaFe<sub>2</sub>O<sub>4</sub> exhibit poor self-healing property during the redox cycle process, even though its crystal phase can be well regenerated, implying that there had been great changes on the surface property, thus, a bad cycle performance was shown in CaFe<sub>2</sub>O<sub>4</sub>. The self-healing property of OC is highly related to the difficulty in oxygen transfer in the lattice. For Ni, Co and Ba, they all have vacant d-orbit, and the orbit can effectively lower the oxygen transfer energy by providing electron acceptor for lattice O, facilitating the regeneration of the crystal structure during the redox cycle process. As a result, NiFe<sub>2</sub>O<sub>4</sub>, CoFe<sub>2</sub>O<sub>4</sub> and BaFe<sub>2</sub>O<sub>4</sub> exhibit excellent cycle performance. Furthermore, the high resolution XPS spectra of O1s were shown in Fig.S 3, and the O1s results also support the aforementioned discussion.

## 3.4. DFT calculation

### 3.4.1. Lattice oxygen property

Based on the H<sub>2</sub>-pulse and XPS results, it can be concluded that there are primarily two types of O in AB<sub>2</sub>O<sub>4</sub>: surface O and lattice O. During the CLPH process, CO selectivity is mainly affected by the amount of surface O, the less O (more oxygen vacancy) in surface, the higher CO selectivity will obtain. And the cycle performance is largely affected by the self-healing property, which in turn is determined by the oxygen

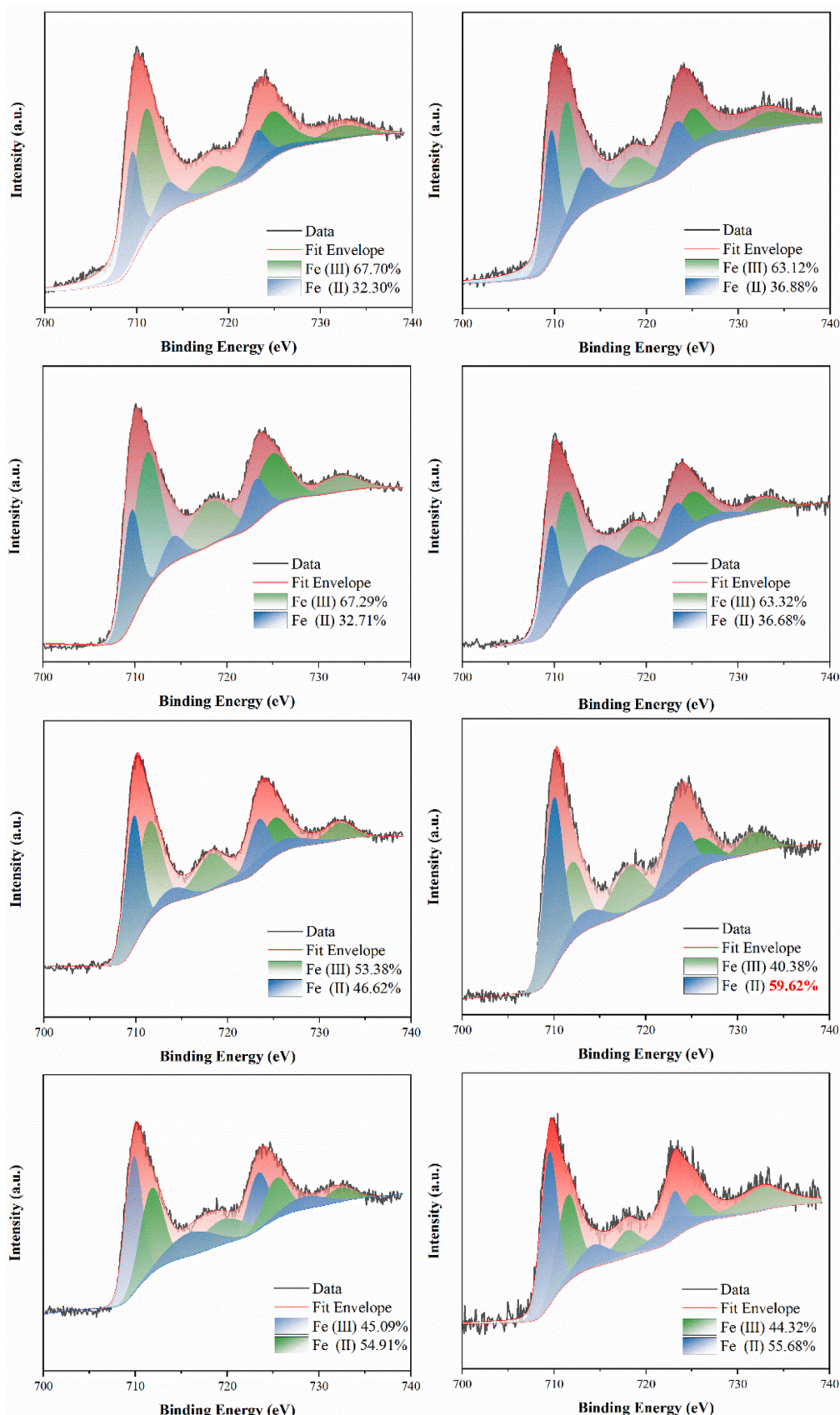


**Fig. 10.** High-resolution XPS spectra of the Fe2p peaks for the fresh and 5-cycled OCs. (a) Fresh NiFe<sub>2</sub>O<sub>4</sub>, (b) 5-cycled NiFe<sub>2</sub>O<sub>4</sub>, (c) Fresh CoFe<sub>2</sub>O<sub>4</sub>, (d) 5-cycled CoFe<sub>2</sub>O<sub>4</sub>, (e) Fresh CaFe<sub>2</sub>O<sub>4</sub>, (f) 5-cycled CaFe<sub>2</sub>O<sub>4</sub>, (g) Fresh BaFe<sub>2</sub>O<sub>4</sub>, (h) 5-cycled BaFe<sub>2</sub>O<sub>4</sub>.

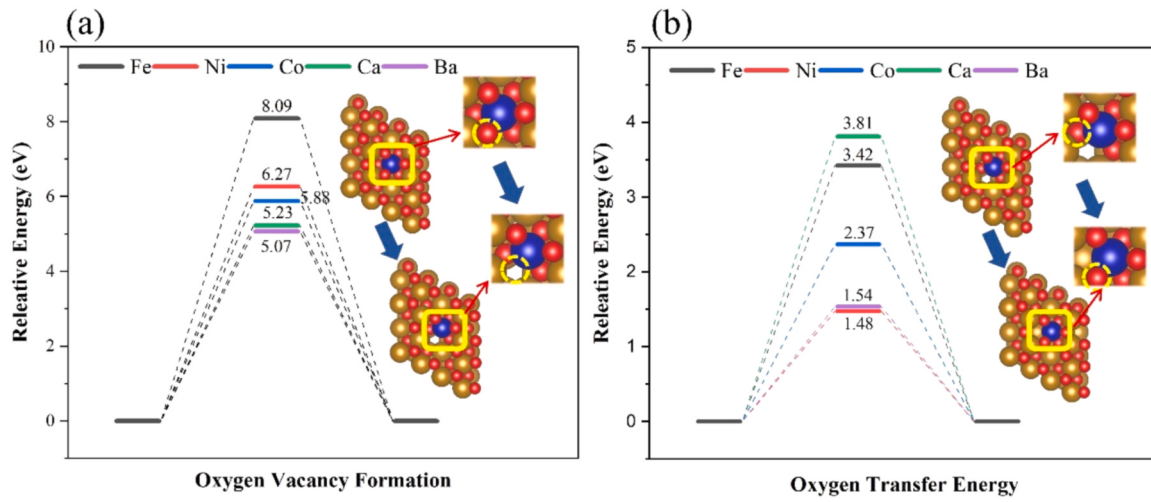


Fig. 11. The differences of lattice oxygen property. (a) The formation energy of oxygen vacancy, (b) The transfer energy of lattice oxygen.

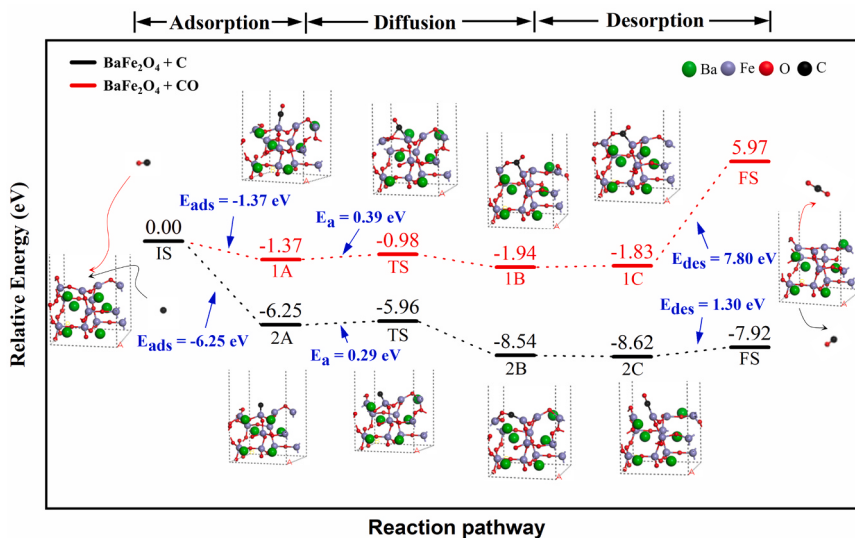


Fig. 12. The energy differences between reaction of  $\text{BaFe}_2\text{O}_4$  with C and CO.

transfer capacity of OC, the easier the oxygen transfer in the lattice, the better the redox performance. To further validate these findings, the oxygen vacancy formation energy and oxygen transfer energy of  $\text{Fe}_3\text{O}_4$  and A (Ni/Co/Ca/Ba) doped  $\text{Fe}_3\text{O}_4$  (one Fe atom replaced by A) were computed using DFT method. The calculation results were shown in Fig. 11. As shown in Fig. 11a, after heteroatom doping, the oxygen vacancy formation energy all decreased, and the oxygen vacancy formation energy follow the order of Ba < Ca < Co < Ni, more oxygen vacancy equals higher CO selectivity, and this order not only resembled with the results of Ellingham diagram, but also matched the CO selectivity results in fixed bed experiments. Additionally, according to the oxygen transfer energy shown in Fig. 11b, it is evident that after Ni/Co/Ba doping, the oxygen transfer energy significantly decreased, indicating a better self-healing property during the redox cycles. However, for Ca-doped OC, its oxygen transfer energy even exceeded that of the  $\text{Fe}_3\text{O}_4$ , which means a worse lattice O transfer capacity, and these results are well consistent with the poor cycle performance of  $\text{CaFe}_2\text{O}_4$  in cycle experiments.

#### 3.4.2. CO selectivity

In order to further interpret the high CO selectivity of  $\text{BaFe}_2\text{O}_4$ , the reaction pathway of  $\text{BaFe}_2\text{O}_4$  with C and CO was calculated by DFT method. The atomic configurations and corresponding relative energy at

different states along the pathway were shown in Fig. 12. The reaction pathway of  $\text{BaFe}_2\text{O}_4$  includes three steps: the adsorption of the reactant, the diffusion of the reactant atoms and the desorption of product. By comparing the energy of these three steps, it can be inferred that the desorption of  $\text{CO}/\text{CO}_2$  products are the rate determining step. For adsorption energy, the adsorption energy of C on  $\text{BaFe}_2\text{O}_4$  (1 1 0) is lower than that of CO, indicating that C is more likely to adsorb on  $\text{BaFe}_2\text{O}_4$ . After reactant adsorption, the adsorbed C atom gradually approached to the nearest O atom and form the complex of  $\text{CO}^*$  (2B) and  $\text{OCO}^*$  (1B) by overcoming an activation energy of 0.29 eV and 0.39 eV, respectively. Finally, the desorption energy of  $\text{CO}_2$  (7.80 eV) is higher than that of CO (1.30 eV), signifying that the desorption of  $\text{CO}_2$  is harder than that of CO, making CO the primary product. In summary, DFT calculation makes it clear that the reaction of  $\text{BaFe}_2\text{O}_4$  and C (generating CO) is more likely to occur than that of  $\text{BaFe}_2\text{O}_4$  and CO (generating  $\text{CO}_2$ ), this effectively explains the excellent CO selectivity of  $\text{BaFe}_2\text{O}_4$ .

## 4. Conclusion

A new chemical looping partial oxidation of biomass char and hydrogen generation process was proposed, this process was expected to generate inherently separated CO-rich gas and high purity of  $\text{H}_2$ . Four

$\text{MFe}_2\text{O}_4$  ( $\text{M}=\text{Ni, Co, Ca, Ba}$ ) OC was chosen according to the modified Ellingham diagram, and the actual redox, cycle performance and reaction mechanism of these OCs during this process was comprehensively investigated. Such conclusions were obtained as followed:

- (1) Reactivity of fresh OC with char decreased in the order of  $\text{NiFe}_2\text{O}_4 > \text{CoFe}_2\text{O}_4 > \text{BaFe}_2\text{O}_4 > \text{CaFe}_2\text{O}_4$ , the purity of  $\text{H}_2$  in SR also followed the same order.  $\text{H}_2$  yield of the fresh OC decreased with the order of  $\text{CoFe}_2\text{O}_4 > \text{NiFe}_2\text{O}_4 > \text{CaFe}_2\text{O}_4 > \text{BaFe}_2\text{O}_4$ . CO selectivity of fresh OC decreased with the order of  $\text{BaFe}_2\text{O}_4 > \text{CaFe}_2\text{O}_4 > \text{CoFe}_2\text{O}_4 \approx \text{NiFe}_2\text{O}_4$ .
- (2) After reacting with biomass char, only  $\text{BaFe}_2\text{O}_4$  can be easily regenerated after reacting with steam, which will decrease the equipment investment and operation risk.
- (3)  $\text{BaFe}_2\text{O}_4$ ,  $\text{CoFe}_2\text{O}_4$  and  $\text{NiFe}_2\text{O}_4$  all show an excellent cycle performance,  $\text{CaFe}_2\text{O}_4$  encounters a dramatic deactivation after the first cycle, the deactivation of  $\text{CaFe}_2\text{O}_4$  is owing to the bad self-healing property which induced by the bad O transfer capacity in lattice.
- (4) The DFT calculation results indicated that the adsorption of CO on  $\text{BaFe}_2\text{O}_4$  (1 1 0) is harder than that of C, and the desorption of CO is easier than that of  $\text{CO}_2$ , thus  $\text{BaFe}_2\text{O}_4$  exhibit an excellent selectivity for CO.

Of all the valuation,  $\text{BaFe}_2\text{O}_4$  is deemed as an ideal OC for the proposed CLPH process.

#### CRediT authorship contribution statement

**Liu Zheyu:** Data curation, Funding acquisition. **Miao Hengyang:** Investigation. **Bai Jin:** Software. **Huang Jiejie:** Conceptualization. **Wang Zhiqing:** Funding acquisition, Writing – review & editing. **Sun Haochen:** Writing – original draft. **Fang Yitian:** Conceptualization, Funding acquisition, Methodology. **Chen Chengmeng:** Software.

#### Declaration of Competing Interest

The authors declare that they have no known competing financial interests or personal relationships that could have appeared to influence the work reported in this paper.

#### Data Availability

The authors do not have permission to share data.

#### Acknowledgments

The work is financially supported by the National Science Foundation of China (22378410), the National Key Research and Development Program of China (2021YFC1808900, 2022YFB4101604), the Chinese Academy of Sciences (CAS) Project for Young Scientists in Basic Research (YSBR-028), the Independent Innovation Fund Project of Institute of Coal Chemistry Chinese Academy of Sciences: Sciences-Basic Research Project (SCJC-WRW-2022-18), the Major Special Deployment Topics of Shanxi Province (202005D121002), Youth Innovation Promotion Association (2014156) and the CAS/SAFEA International Partnership Program for Creative Research Teams.

#### Appendix A. Supporting information

Supplementary data associated with this article can be found in the online version at [doi:10.1016/j.apcatb.2024.123729](https://doi.org/10.1016/j.apcatb.2024.123729).

#### References

- [1] S.K. Sansaniwal, K. Pal, M.A. Rosen, S.K. Tyagi, Recent advances in the development of biomass gasification technology: a comprehensive review, *Renew. Sustain. Energy Rev.* 72 (2017) 363–384.
- [2] X. Ji, X. Long, A review of the ecological and socioeconomic effects of biofuel and energy policy recommendations, *Renew. Sustain. Energy Rev.* 61 (2016) 41–52.
- [3] S. Ersan, J.O. Park, Light-Independent Biological Conversion of  $\text{CO}_2$ , *Joule* 4 (2020) 2047–2051.
- [4] X. Zhao, H. Zhou, V.S. Sikarwar, M. Zhao, A.-H.A. Park, P.S. Fennell, L. Shen, L.-S. Fan, Biomass-based chemical looping technologies: the good, the bad and the future, *Energy Environ. Sci.* 10 (2017) 1885–1910.
- [5] M. Gattrell, N. Gupta, A. Co, Electrochemical reduction of  $\text{CO}_2$  to hydrocarbons to store renewable electrical energy and upgrade biogas, *Energy Convers. Manag.* 48 (2007) 1255–1265.
- [6] W.H. Chen, B.J. Lin, Hydrogen and synthesis gas production from activated carbon and steam via reusing carbon dioxide, *Appl. Energy* 101 (2013) 551–559.
- [7] E. Shayan, V. Zare, I. Mirzaee, Hydrogen production from biomass gasification; a theoretical comparison of using different gasification agents, *Energy Convers. Manag.* 159 (2018) 30–41.
- [8] F.Y. Chen, C.F. Wu, L.S. Dong, A. Vassallo, P.T. Williams, J. Huang, Characteristics and catalytic properties of  $\text{Ni}/\text{CaAlO}_x$  catalyst for hydrogen-enriched syngas production from pyrolysis-steam reforming of biomass sawdust, *Appl. Catal. B: Environ.* 183 (2016) 168–175.
- [9] Z. Cui, W. Tian, H. Zhang, Q. Guo, Multi-scale modeling and control of chemical looping gasification coupled coal pyrolysis system for cleaner production of synthesis gas, *J. Clean. Prod.* 299 (2021) 126903.
- [10] T. Song, L. Shen, Review of reactor for chemical looping combustion of solid fuels, *Int. J. Greenh. Gas. Control* 76 (2018) 92–110.
- [11] W.H. Chen, K.H. Chen, A.T. Ubando, W.J. Lee, M.H. Chio, Redox degrees of iron-based oxygen carriers in cyclic chemical looping combustion using thermodynamic analysis, *Chem. Eng. J.* 426 (2021) 130834.
- [12] S. Yang, T. Zhang, Y. Yang, B. Wang, J. Li, Z. Gong, Z. Yao, W. Du, S. Liu, Z. Yu, Molybdenum-based nitrogen carrier for ammonia production via a chemical looping route, *Appl. Catal. B: Environ.* 312 (2022) 121404.
- [13] A. Joshi, V. Shah, P. Mohapatra, S. Kumar, R.K. Joshi, M. Kathe, L. Qin, A. Tong, L.-S. Fan, Chemical looping-A perspective on the next-gen technology for efficient fossil fuel utilization, *Adv. Appl. Energy* 3 (2021) 100044.
- [14] Z. Huang, F. He, Y. Feng, K. Zhao, A. Zheng, S. Chang, H. Li, Synthesis gas production through biomass direct chemical looping conversion with natural hematite as an oxygen carrier, *Bioresour. Technol.* 140 (2013) 138–145.
- [15] F. He, Z. Huang, G. Wei, K. Zhao, G. Wang, X. Kong, Y. Feng, H. Tan, S. Hou, Y. Lv, G. Jiang, Y. Guo, Biomass chemical-looping gasification coupled with water/ $\text{CO}_2$ -splitting using  $\text{NiFe}_2\text{O}_4$  as an oxygen carrier, *Energy Convers. Manag.* 201 (2019) 112157.
- [16] Z. Sun, S. Chen, C.K. Russell, J. Hu, A.H. Rony, G. Tan, A. Chen, L. Duan, J. Boman, J. Tang, T. Chien, M. Fan, W. Xiang, Improvement of  $\text{H}_2$ -rich gas production with tar abatement from pine wood conversion over bi-functional  $\text{Ca}_2\text{Fe}_2\text{O}_5$  catalyst: Investigation of inner-looping redox reaction and promoting mechanisms, *Appl. Energy* 212 (2018) 931–943.
- [17] S. Chen, Q. Shi, Z. Xue, X. Sun, W. Xiang, Experimental investigation of chemical-looping hydrogen generation using  $\text{Al}_2\text{O}_3$  or  $\text{TiO}_2$ -supported iron oxides in a batch fluidized bed, *Int. J. Hydrol. Energy* 36 (2011) 8915–8926.
- [18] I. Wang, G. Ji, Y. Turap, H. Nie, Z. Li, M. Zhao, W. Wang, A short-cut chemical looping hydrogen generation system by using iron-based material from steel industry, *Chem. Eng. J.* 394 (2020) 124882.
- [19] S. Ma, M. Li, G. Wang, L. Zhang, S. Chen, Z. Sun, J. Hu, M. Zhu, W. Xiang, Effects of Zr doping on  $\text{Fe}_2\text{O}_3/\text{CeO}_2$  oxygen carrier in chemical looping hydrogen generation, *Chem. Eng. J.* 346 (2018) 712–725.
- [20] J. Adanez, A. Abad, F. Garcia-Labiano, P. Gayan, L.F. de Diego, Progress in Chemical-Looping Combustion and Reforming technologies, *Prog. Energy Combust. Sci.* 38 (2012) 215–282.
- [21] M. Zhu, S. Chen, S. Ma, W. Xiang, Carbon formation on iron-based oxygen carriers during  $\text{CH}_4$  reduction period in Chemical Looping Hydrogen Generation process, *Chem. Eng. J.* 325 (2017) 322–331.
- [22] Z. Wang, Z. Gong, Y. Turap, Y. Wang, Z. Zhang, W. Wang, Renewable hydrogen production from biogas using iron-based chemical looping technology, *Chem. Eng. J.* 429 (2022) 132192.
- [23] J. Zhang, F. Li, Coke-resistant  $\text{Ni}/\text{SiO}_2$  catalyst for dry reforming of methane, *Appl. Catal. B: Environ.* 176–177 (2015) 513–521.
- [24] J. Zhang, T. He, Z. Wang, M. Zhu, K. Zhang, B. Li, J. Wu, The search of proper oxygen carriers for chemical looping partial oxidation of carbon, *Appl. Energy* 190 (2017) 1119–1125.
- [25] R. Siriwardane, J. Riley, H. Tian, G. Richards, Chemical looping coal gasification with calcium ferrite and barium ferrite via solid-solid reactions, *Appl. Energy* 165 (2016) 952–966.
- [26] J. Riley, R. Siriwardane, H. Tian, W. Benincosa, J. Poston, Kinetic analysis of the interactions between calcium ferrite and coal char for chemical looping gasification applications: Identifying reduction routes and modes of oxygen transfer, *Appl. Energy* 201 (2017) 94–110.
- [27] D.D. Miller, R. Siriwardane,  $\text{CaFe}_2\text{O}_4$  oxygen carrier characterization during the partial oxidation of coal in the chemical looping gasification application, *Appl. Energy* 224 (2018) 708–716.
- [28] J. Chen, K. Zhao, Z. Zhao, F. He, Z. Huang, G. Wei, Identifying the roles of  $\text{MFe}_2\text{O}_4$  ( $\text{M}=\text{Cu, Ba, Ni, and Co}$ ) in the chemical looping reforming of char, pyrolysis gas

- and tar resulting from biomass pyrolysis, *Int. J. Hydrol. Energy* 44 (2019) 4674–4687.
- [29] J. Yan, R. Sun, L. Shen, H. Bai, S. Jiang, Y. Xiao, T. Song, Hydrogen-rich syngas production with tar elimination via biomass chemical looping gasification (BCLG) using BaFe<sub>2</sub>O<sub>4</sub>/Al<sub>2</sub>O<sub>3</sub> as oxygen carrier, *Chem. Eng. J.* 387 (2020) 124107.
- [30] M. Diaz-Somoano, M.R. Martinez-Tarazona, Trace element evaporation during coal gasification based on a thermodynamic equilibrium calculation approach, *Fuel* 82 (2003) 137–145.
- [31] B. Wang, C. Gao, W. Wang, F. Kong, C. Zheng, TGA-FTIR investigation of chemical looping combustion by coal with CoFe<sub>2</sub>O<sub>4</sub> combined oxygen carrier, *J. Anal. Appl. Pyrolysis* 105 (2014) 369–378.
- [32] X. Wang, Z. Chen, M. Hu, Y. Tian, X. Jin, S. Ma, T. Xu, Z. Hu, S. Liu, D. Guo, B. Xiao, Chemical looping combustion of biomass using metal ferrites as oxygen carriers, *Chem. Eng. J.* 312 (2017) 252–262.
- [33] G. Kresse, J. Furthmuller, Efficiency of ab-initio total energy calculations for metals and semiconductors using a plane-wave basis set, *Comput. Mater. Sci.* 6 (1996) 15–50.
- [34] G. Kresse, J. Furthmuller, Efficient iterative schemes for ab initio total-energy calculations using a plane-wave basis set, *Phys. Rev. B* 54 (1996) 11169–11186.
- [35] J.P. Perdew, K. Burke, M. Ernzerhof, Generalized gradient approximation made simple, *Phys. Rev. Lett.* 77 (1996) 3865–3868.
- [36] S. Liu, D. Xiang, Y. Xu, Z. Sun, Y. Cao, Relationship between electronic properties of Fe<sub>3</sub>O<sub>4</sub> substituted by Ca and Ba and their reactivity in chemical looping process: A first-principles study, *Appl. Energy* 202 (2017) 550–557.
- [37] S. Liu, Z. Dong, D. Xiang, Y. Jiang, Q. Tao, Y. Cao, Crossing-link of experimental reducibility tests, XPS characterizations and DFT estimates on ferrite oxygen carriers in CLC, *Appl. Catal. B: Environ.* 238 (2018) 647–655.
- [38] C.L. Muñich, V.J. Aston, R.M. Trottier, A.W. Weimer, C.B. Musgrave, First-Principles Analysis of Cation Diffusion in Mixed Metal Ferrite Spinels, *Chem. Mater.* 28 (2016) 214–226.
- [39] G. Henkelman, B.P. Uberuaga, H. Jonsson, A climbing image nudged elastic band method for finding saddle points and minimum energy paths, *J. Chem. Phys.* 113 (2000) 9901–9904.
- [40] J. Zhang, V. Haribal, F. Li, Perovskite nanocomposites as effective CO<sub>2</sub>-splitting agents in a cyclic redox scheme, *Sci. Adv.* 3 (2017) e1701184.
- [41] S.K. Rakshit, S.C. Parida, Z. Singh, R. Prasad, V. Venugopal, Thermodynamic properties of ternary oxides in the system Ba–Fe–O using solid-state electrochemical cells with oxide and fluoride ion conducting electrolytes, *J. Solid State Chem.* 177 (2004) 1146–1156.
- [42] L. Zeng, M.V. Kathe, E.Y. Chung, L.-S. Fan, Some remarks on direct solid fuel combustion using chemical looping processes, *Curr. Opin. Chem. Eng.* 1 (2012) 290–295.
- [43] V.P. Haribal, F. He, A. Mishra, F. Li, Iron-Doped BaMnO<sub>3</sub> for Hybrid Water Splitting and Syngas Generation, *ChemSusChem* 10 (2017) 3402–3408.
- [44] S. Luo, L. Zeng, D. Xu, M. Kathe, E. Chung, N. Deshpande, L. Qin, A. Majumder, T.-L. Hsieh, A. Tong, Z. Sun, L.-S. Fan, Shale gas-to-syngas chemical looping process for stable shale gas conversion to high purity syngas with a H<sub>2</sub>: CO ratio of 2: 1, *Energy Environ. Sci.* 7 (2014) 4104–4117.
- [45] X. Li, P. Xu, Y. Zhou, Y. Chen, H. Jia, H. Yu, X. Li, In Situ Hydrogen Temperature-Programmed Reduction Technology Based on the Integrated Microcantilever for Metal Oxide Catalyst Analysis, *Anal. Chem.* 94 (2022) 16502–16509.
- [46] Y.-Y. Chen, M. Guo, M. Kim, Y. Liu, L. Qin, T.-L. Hsieh, L.-S. Fan, Predictive screening and validation on chemical looping oxygen carrier activation by tuning electronic structures via transition metal dopants, *Chem. Eng. J.* 406 (2021) 126729.
- [47] Z. Gao, F. Fu, Z. Zhang, L. Niu, M. Jin, J. Zhang, Z. Zhao, Gd, La co-doped CeO<sub>2</sub> as an active support for Fe<sub>2</sub>O<sub>3</sub> to enhance hydrogen generation via chemical looping water gas shift, *Int. J. Hydrot. Energy* 47 (2022) 22806–22818.
- [48] L.M. Neal, A. Shafiefarhood, F. Li, Dynamic Methane Partial Oxidation Using a Fe<sub>2</sub>O<sub>3</sub>@La<sub>0.8</sub>Sr<sub>0.2</sub>FeO<sub>3-δ</sub> Core–Shell Redox Catalyst in the Absence of Gaseous Oxygen, *ACS Catal.* 4 (2014) 3560–3569.
- [49] F. Donat, C.R. Müller, CO<sub>2</sub>-free conversion of CH<sub>4</sub> to syngas using chemical looping, *Appl. Catal. B: Environ.* 278 (2020) 119328.
- [50] D. Zeng, Y. Qiu, M. Li, L. Ma, D. Cui, S. Zhang, R. Xiao, Spatially controlled oxygen storage materials improved the syngas selectivity on chemical looping methane conversion, *Appl. Catal. B: Environ.* 281 (2021) 119472.
- [51] S. Poulin, R. França, L. Moreau-Bélanger, E. Sacher, Confirmation of X-ray photoelectron spectroscopy peak attributions of nanoparticulate iron oxides, using symmetric peak component line shapes, *J. Phys. Chem. C.* 114 (2010) 10711–10718.
- [52] T. Yamashita, P. Hayes, Analysis of XPS spectra of Fe<sup>2+</sup> and Fe<sup>3+</sup> ions in oxide materials, *Appl. Surf. Sci.* 254 (2008) 2441–2449.
- [53] R. Sun, Y. Xiao, J. Yan, L. Shen, H. Bai, Mechanism study on the high-performance BaFe<sub>2</sub>O<sub>4</sub> during chemical looping gasification, *Fuel* 307 (2022) 121847.